Performance Evaluation of A High Energy Pulsed Plasma Thruster II

IEPC-2005-282

Presented at the 29th International Electric Propulsion Conference, Princeton University,
October 31 – November 4, 2005

Hani Kamhawi*,
NASA Glenn Research Center at Lewis Field, Cleveland, Ohio, 44135

Lynn Arrington†
QSS. Group, Cleveland, Ohio, 44135

and

Eric Pencil‡ and Thomas Haag§
NASA Glenn Research Center at Lewis Field, Cleveland, Ohio, 44135

Abstract: NASA Glenn Research Center (GRC) has evaluated the performance of a pulsed plasma thruster (PPT) at energy levels up to 700 J. Previous testing was performed and reported on a thruster configuration designated *HEPPT1b*. This paper presents test results for evaluating the performance of a different thruster configuration designated *HEPPT2*. The main difference between the two configurations is in the lower transmission line inductance of *HEPPT2* when compared to *HEPPT1b*. *HEPPT2* tests were conducted at capacitance values of 100 µF, 180 µF and 260 µF for energy levels ranging from 100 J to 700J. Discharge current waveforms, polytetrafluoroethylene (PTFE) mass loss, and impulse-bit magnitudes were measured and the thrust efficiency and specific impulse were computed. Test results indicated that at a given operating condition (both capacitance and energy), *HEPPT2* performance was only 3-5% higher than *HEPPT1b*. The highest specific impulse of 3940 sec and thrust efficiency of 36% were attained by *HEPPT2* at a capacitance of 260 µF and discharge energy of 700 J.

Nomenclature

AR	=	Planar electrodes aspect ratio
C	=	Capacitance, Farad
E	=	Energy of PPT discharge capacitor, J
f	=	Planar electrodes inductance fringe factor
g	=	Gravitational acceleration, 9.81 m/sec^2
h	=	Inter-electrode spacing, cm
I_{bit}	=	Impulse-bit, µN.sec
I_{mag}	=	Electromagnetic component of impulse bit
$I(t)$	=	Discharge current, A

* Aerospace Engineer, Electric Propulsion Branch, 21000 Brookpark Rd/Ms 16-1, AIAA Senior Member.
† Mechanical Engineer, Electric Propulsion Branch, 21000 Brookpark Rd/Ms 301-3, AIAA Senior Member.
‡ Electrical Engineer, Electric Propulsion Branch, 21000 Brookpark Rd/Ms 301-3, Associate AIAA Fellow.
§ Mechanical Engineer, Electric Propulsion Branch, 21000 Brookpark Rd/Ms 301-3, AIAA Member.

I_{sp} = Specific impulse, sec
L = Inductance, Henry
$m_{ablated}$ = Mass loss per pulse of polytetrafluoroethylene, μg
T = Pulse period, sec
w = Electrode width, cm
x = Axial distance along electrode length, cm
η = Thrust efficiency, %

I. Introduction

Pulsed plasma thrusters (PPTs) are simple and robust devices that have been used for station keeping and attitude control on a number of spacecraft.[1,2] However, PPTs suffer from low thrust efficiency. Typical PPT thrust efficiencies have been below 15% for energy levels below 50 J, with the low thrust efficiency mainly attributed to poor utilization of the ablated solid propellant. A number of studies have been performed to research improving PPT thrust efficiency, mainly by varying the electrodes and propellant configurations and by implementing various thruster electrical circuits, but these efforts did not achieve the desired 2× improvements in PPT thrust efficiency performance in the energy range below 70 J.[3,4]

Another approach of demonstrating a higher PPT thrust efficiency is by operating the thruster at higher energy levels. Several research efforts investigated the performance of PPTs at energy levels above 100 J. In the 1970's Palumbo and Guman constructed a 450 J PPT that utilized 12 oil impregnated mylar capacitors rated at 9 μF and 8kV. In these tests two electrode/propellant configurations were tested: breech–fed and side-fed. Palumbo and Guman demonstrated that at 450 J a breech-fed electrode geometry with Teflon propellant and planar ablation surfaces can achieve a thrust efficiency of 53% with a specific impulse of 5170 sec.[5,6,7] In 1997, researchers in Russia evaluated the performance of PPTs at energy levels of 100 J and 150 J. Antropov et al. reported that the thrust efficiency of a 100 J dielectric erosion PPT with plane bars was between 10% and 13%. To increase PPT thrust efficiency Antropov suggested the application of a "long" discharge current pulse.[8] In 2001, Popov et al., later demonstrated the operation of a 40 J to150 J ablation pulsed plasma thruster (APPT). At 150 J the APPT had a thrust efficiency of 28% and a specific impulse of 2100 sec. This higher thrust efficiency was achieved with a non-reversing discharge current waveform.[9] In 2002, Kazeev et al. demonstrated the operation of a 100 J PPT at a thrust efficiency of 24% and a specific impulse of 1800 sec. The discharge current waveform was sinusoidal with a peak current value of ~ 28 kA and a first-half period of ~ 9 μsec, twice the typical PPT half-period.[10] Antropov et al. demonstrated an APPT with a thrust efficiency of ~30% at 150 J.[11] Finally, in 2003 Pencil and Kamhawi reported on the performance of a 100 J class PPT. The PPT demonstrated a thrust efficiency of ~14% at an energy level of 140 J when polytetrafluoroethylene (PTFE) was utilized as propellant. Higher thrust efficiencies of 17% were obtained when 2% carbon-impregnated PTFE was utilized.[12]

The results presented in this paper are a continuation of testing that was performed and presented on the evaluation of the performance of a 100 to 700 J class PPTs.[13] The work presented here reports on the testing result for the second configuration whose testing was only initiated during the last report. The goal of this additional testing aims to determine if the results obtained by Palumbo and Guman[5,6] can be duplicated. Once that goal is at hand, additional optimization on the high energy PPT configuration to achieve additional performance improvements will be pursued.[14] Additionally, once higher PPT thrust efficiencies have been demonstrated, a more rigorous interrogation of the propellant surface temperatures and plasma properties in the inter-electrode region and in the thruster plume and numerical simulations using the MACH2 code will be performed to elucidate the physics underlying improved PPT performance at higher energy levels.[15,16,17]

II. Experimental Facilities and Apparatus

A. Vacuum Facility

Tests were performed at NASA Glenn Research Center (GRC) in vacuum facility 3 (VF-3) in the Electric Propulsion Research Building (EPRB). The vacuum facility is evacuated with four oil diffusion pumps (ODP) that are backed by a roughing pump; the ODPs have a pumping speed of 80,000 liter/sec at 0.05 mPa (1 μTorr) of air. The vacuum chamber is 1.5 m in diameter and is 4.5 m long. Typical facility background pressure during single pulse PPT testing was 0.1 mPa (2 μTorr) as measured with an ion gauge.

B. Experimental PPT Hardware

Testing performed for this paper was performed with High Energy PPT2 (*HEPPT2*), which is the second configuration of a high energy PPT that was constructed and tested. *HEPPT2* utilized commercially available

rectangular mica foil capacitors. The capacitors used in testing had a capacitance of 10 μF each and were rated at 2500 VDC. The capacitor dimensions were 12.7 cm (H) × 5.0 cm (W) × 8.0 cm (D) and weighed 1.19 kg each.

The copper ground transmission line was 0.16 cm thick, 80 cm long and 30.5 cm wide. The capacitors' ground terminals were attached together with two 81 cm (L) × 2.5 cm (W) × 0.5 cm (H) copper bars which were in turn connected to the ground transmission copper sheet; the hot copper transmission line was 0.43 cm thick U-channel of dimensions 82 cm (L) × 5 cm (W) × 1.5cm (H). Plexiglass supports were used to support the weight of the ground and high voltage transmission lines. Configuration *HEPPT2* allows for the installation of a maximum of 26 10 μF capacitors in parallel in 13 rows for a total capacitance of 260 μF with row 1 being furthest away from electrode assembly and row 13 being closest to electrode assembly. Figure 1 presents a picture of *HEPPT2* partially disassembled showing 13 rows of capacitors and the copper hot and ground transmission lines.

HEPPT2 electrodes were fabricated from oxygen-free copper. They were 1.91 cm wide and its exposed length was 4.1 cm. These dimensions were based on electrode configurations tested by Palumbo and Guman.[5,6] The insulating labyrinth inter-electrode nozzle was fabricated from high temperature machinable glass ceramic pieces which are more ablation resistant. No propellant feed system was required during testing since only a small number of pulses were required to evaluate PPT performance. Figure 2 shows a picture of the inter-electrode region of *HEPPT2*.

The main differences between *HEPPT1b* and *HEPPT2* configurations are in the electrical transmission line layout. Details of configuration *HEPPT1b* setup can be found in reference 13. Figures 3 and 4 present backview pictures detailing the cross sectional layout of *HEPPT1b* and *HEPPT2*, respectively. *HEPPT2* design and fabrication was initiated after testing with *HEPPT1b* indicated that transmission line inductance was limiting the peak discharge current magnitudes, thereby affecting thruster performance. The *HEPPT2* design aimed to reduce transmission line inductance and improve thruster performance. Analysis presented in reference 13, found that *HEPPT2* transmission line layout decreased the circuit inductance by a factor of ~ 6 from the *HEPPT1b* design.

A 600 W commercially available high voltage power supply (0-200 mA, 0-3000 V) was used to charge the PPT capacitors. For PPT discharge initiation, a commercially available annular semi-conductor spark plug of 1.27 cm diameter was attached directly to the ground electrode via a 1.27 cm hole located 0.13 cm from propellant face. The discharge initiation circuit used in these tests was a commercially available ignition excitor typically used to ignite combustion chambers of airplane engines.

C. Thrust Stand

A torsional-type thrust stand was used to perform thrust measurements.[18] The thrust stand was used to determine impulse-bit as a function of thrust stand deflection, spring stiffness, and natural frequency. In-situ calibration weights were used to apply a known force to determine the deflection of the thrust stand. The thrust stand had a 2% uncertainty in the impulse-bit measurement. For testing with the high energy PPT only single impulses were measured. The impulse-bit per shot was calculated from an average of thirty pulses to average out shot-to-shot variation in the thruster performance. Typical shot-to-shot variation was ~ 5%. Figure 5 shows *HEPPT2* mounted on the NASA GRC PPT thrust stand in VF-3.

D. Test Matrix

Testing of configuration *HEPPT2* tests was performed at a thruster capacitance of 100, 180, and 260 μF. Table 1 lists the energy levels at which testing was performed for the different thruster capacitance values. Table 2 lists the corresponding charging voltages at the different test points. For a typical PPT firing, it was observed that the thruster's capacitors contained a residual charge of around 100 V which equates to 1.3 J at a thruster capacitance of 260 μF.

III. Experimental Results and Analysis

The following section presents the experimental results and analysis from all the testing that was performed to date for configuration *HEPPT2*. The experimental results include current waveforms, PTFE mass loss, and impulse-bit magnitudes for the different thruster configurations and energy levels that were tested. PPT thrust efficiency and specific impulse values are presented and analyzed. Typical error bars are included in each plot for one of the cases that were tested. Finally, zeroth-order modeling is performed to gain better insights into the thruster's performance.

A. Experimental Current Waveforms

The experimental current waveforms for *HEPPT2* tests were measured with a Rogowski loop. The calibrated Rogowski loop output had a sensitivity of 5010 A/V into 50 Ohms. To confirm that the Rogowski loop calibration

number is accurate, the experimental current waveforms were integrated and the value of the integral was compared to the capacitor bank total charge ($Q=CV_0$). Results of the analysis indicated that for all the experimentally measured current waveforms the integral of the current waveform was within 5-8% of the capacitor bank initial total charge. Figure 6 presents the discharge current waveforms for *HEPPT2* operation at 100 μF (5 rows of capacitors) for the different energy levels, the discharge current waveforms were a sinusoidal under-damped current waveform. Peak discharge current magnitudes of 29.6 kA, 45 kA, and 54.6 kA were attained at energy levels of 100 J, 200 J, and 300 J, respectively. Figure 7 presents the discharge current waveforms for *HEPPT2* operation at 180 μF (9 rows of capacitors. Peak discharge current magnitudes of 25.6 kA, 39.6 kA, 51.1 kA, and 64 kA were attained at energy levels of 100 J, 200 J, 300 J, and 450 J, respectively. Figure 8 presents the discharge current waveforms for *HEPPT2* operation at 260 μF (13 rows of capacitors). Peak discharge current magnitudes of 22.3 kA, 33.3kA, 42.2 kA, 53.6 kA, and 64 kA were attained at energy levels of 100 J, 200 J, 300 J, 450 J, and 700 J, respectively.

The experimental current waveforms reveal that as the thruster capacitance is increased the current waveform period ($T=2\pi\sqrt{(LC)}$) increases, however, $(dI/dt)_{t=0}$ remains the same since the section inductance and capacitance have not changed. At a given thruster energy, increasing the thruster capacitance, results in a current waveform with higher current peak values mainly due to the higher charging voltages at the lower thruster capacitances

B. PTFE Mass Loss Measurements

The total number of pulses applied to achieve a representative PTFE mass loss per pulse varied depending of the PPT discharge energy level. For discharge energy levels of 100 J, 200 J, 300 J, 450 J, and 700 J, the number of pulses applied was approximately 1000, 500, 500, 300, and 300, respectively. The PTFE propellant bar weight was approximately 154 g. Typical PTFE propellant total mass loss ranged from approximately 70 mg to 100 mg. PTFE mass measurements were performed with an electronic balance that had an accuracy of 1 mg. In all PTFE mass loss measurements it is found that PTFE mass loss magnitudes are directly proportional to PPT discharge energy. Least-square fits which included the origin were applied to PTFE mass loss. No investigation was performed to evaluate the effect of PPT pulse repetition rate on PTFE mass loss magnitudes since that was beyond the scope of this preliminary evaluation of high energy PPTs.

Figure 9 presents PTFE mass loss results for the test matrix listed in Table 1. For a thruster capacitance of 100 μF, 180 μF, and 260 μF, the least square fit equations were 0.83*E μg/J, 0.66*E μg/J, and $0.75*E-0.0004*E^2$, respectively. For a given energy level the PTFE mass loss magnitudes were consistently higher for the case of the lowest thruster capacitance. Since higher peak current occur at the lower capacitance values for a given energy level, higher heat fluxes ($\alpha \int I^2(t)$) are also present. This contributes to greater PTFE heating which results in PTFE surface temperatures resulting in propellant decomposition above and beyond what is required for efficient thruster operation. As the thruster capacitance is increased along with its discharge energy, its mass utilization becomes more efficient and the decomposition and ablation of PTFE after the current pulse is reduced, this can possibly explain the second order form of the linear fit at a capacitance of 260 μF.

C. Impulse-Bit Measurements

For all impulse-bit measurements, it is found that impulse-bit is directly proportional to discharge energy. Least-square linear fits, which included the origin were applied to the PPT impulse-bit results. Figure 10 presents impulse bit results for the test matrix listed in Table 1. For a thruster capacitance of 100 μF, 180 μF, and 260 μF, the least square fit equations were 16.7*E μNsec/J, 17.4*E μNsec/J, and 18.6*E μNsec/J, respectively. It is noted that impulse-bit magnitudes increased as the thruster capacitance was increased for a given energy level. This can be attributed to the change in the current waveform to a critically-damped from an under-damped form which results in more efficient transfer of the discharge energy to the plasma and thus enhanced electromagnetic acceleration.

C. Specific Impulse and Thrust Efficiency

To compute the PPT thrust efficiency and specific impulse, the following equations are used:

$$I_{sp} = \frac{I_{bit}}{mg} \tag{1}$$

$$\eta = \frac{I^2_{bit}}{2mE} \tag{2}$$

Figures 11 and 12 present the specific impulse and thrust efficiency magnitudes, respectively. Figures 11 and 12 indicate that, in general, thruster performance improved as the thruster's discharge energy was increased. Higher specific impulse and thrust efficiencies were attained for a thruster capacitance of 260 μF when compared to the

lower capacitance cases. In addition, comparing the performance results for *HEPPT1b* (reference 13) with *HEPPT2* indicates that operating with a lower circuit inductance enhanced thruster performance only by 3-5%.

D. Analysis

A zeroth-order analysis was performed to gain additional insights into the PPT performance. It has been shown by previous work that[19]

$$m_{ablated} \propto \int_{o}^{t} I^2(t)dt \tag{3}$$

Figure 13 presents a plot of $m_{ablated}$ vs. $\int I^2(t)dt$ for thruster operation at the different capacitance values and energy levels indicating a linear trend. Figure 13 shows that, in general, at a given thruster discharge energy, higher $\int I^2(t)dt$ magnitudes are attained for lower thruster capacitance, that is mainly attributed to the higher peak currents attained at those energy levels. Next to compute the electromagnetic components of the total impulse bit the following equation is used:[19]

$$I_{mag} = \frac{1}{2}\frac{dL}{dx}\int_{o}^{t} I^2(t)dt \tag{4}$$

where[20]

$$L(x) = f\ \frac{\mu_o h}{w}x \tag{5}$$

hence

$$I_{mag} = f\frac{\mu_o h}{2w}\int_{o}^{t} I^2(t)dt \tag{6}$$

For the electrode geometry with an AR of 4, the inductance fringe factor according to reference 20 is ~ 0.2. By plugging the experimental current waveforms, electrode geometry parameters, and the *f* value into equation 3, it is found that the electromagnetic $\boldsymbol{J}\times\boldsymbol{B}$ Lorentz force is almost 2× the measured impulse bit. This indicates that loss of plasma and plasma momentum and energy is occurring due to viscous drag, condensation on solid surface, and disruptions of plasma-slug integrity by plasma instabilities values.[21]

Finally, no estimates or computation of the fraction of the mass the is accelerated electromagnetically were attempted here since no data exists in the literature as to the magnitude of the exhaust speeds encountered in higher energy PPTs. Using the values of 40 km/s reported earlier was not implemented here since those PPTs operated at energies of ~ 40 J.

IV. Conclusions

The evaluation of the performance of *HEPPT2* has been completed. Specific impulse and thrust efficiency of a 700 J class PPT has been reported. Results from this series of testing for configuration *HEPPT2* indicate that reducing the thruster inductance, although substantially altered the discharge current waveform, it did not improve the thruster performance over what has been reported for configuration *HEPPT1b*.[13] Operating *HEPPT2* at a thruster capacitance of 100 μF and 180 μF and 260 μF did not yield substantial performance improvements over *HEPPT1b*.

At a thruster discharge energy of 700 J, specific impulse of ~ 4000 sec and thrust efficiency of ~35% were achieved for a thruster capacitance of 260 μF. At a discharge energy of 450 J, the specific impulse and thrust efficiency values of 3550 sec and 33% sec are substantially lower than the 5170 sec and 53% attained by Palumbo and Guman for the same energy level.[5,6]

Acknowledgments

This work has been supported by the Energetics Heritage Project, formerly an element of the Aerospace Technology Enterprise's (Code R) Mission and Science Measurement Technology theme. The authors would like to acknowledge the efforts of Dennis Rogers from the Test Installation division for his fabrication and assembly of the high energy pulsed plasma thruster. Additionally, the efforts of James Coy, and Donna Neville from the Test Installation Division are greatly appreciated.

References

[1]Kowl, S.J., "Post Launch Results of the Tip Spacecraft Pulsed Plasma Microthrusters," CPIA Publication No. 315, March 1980.
[2]Benson, S.W., Arrington, L.A., Hoskins, W.A., and Meckel, N.J., "Development of a PPT for the EO-1 Spacecraft," AIAA paper 99-2276, June 1999.
[3]Vondra, J.R., and Thomassen, K.I, "Performance Improvements in Solid Fuel Microthrusters," *J. Spacecraft* Vol. 9, No. 10, October 1972, pp. 738-742.
[4]Kamhawi, H., and Turchi, P.J., "Design, Operation, and Investigation of an Inductively-Driven Pulsed Plasma Thruster," AIAA paper 98-3804.
[5]Palumbo, D.J., and Guman, W.J., "Pulsed Plasma Propulsion Technology," AFRPL-TR-73-79, interim report, September 1973.
[6]Palumbo, D.J., and Guman, W.J., "Effects of Propellant and Electrode Geometry on Pulsed ablative Plasma Thruster Performance," *J. Spacecraft*, Vol. 13, No. 3, March 1976, pp 163-167.
[7]Palumbo, D.J., and Guman, W.J., "Propellant Sidefeed-Short Pulse Discharge Thruster Studies," NASA CR-112035, January 1972.
[8]Antropov, N., et al., "Parameters of Plasmoids Injected by PPT," AIAA paper 1997-2921, July 1997.
[9]Popov, G., et al., "Experimental Study of Plasma Parameters in High Efficiency Pulsed Plasma Thrusters," IEPC paper 01-163.
[10]Kazeev, M.N., et al., "Dynamics and Distribution of Electron Density in the Channel of Pulsed Plasma Thruster," AIAA paper 2002-4119, July 2002.
[11]Antropov, N., et al., "Development and Refinement of Highly Efficient 150 J APPT," IEPC paper 03-061.
[12]Pencil, E.J., and Kamhawi, H., "Alternate Propellant Evaluation for 100 joule-class Pulsed Plasma Thrusters," AIAA paper 2003-5171, July 2003.
[13]Kamhawi, H., et al., "Performance Evaluation of a High Energy Pulsed Plasma Thruster," AIAA-
[14]Pencil, E.J., Kamhawi, H., Gilland, J.H., and Arrington, L.A., "Overview of Advanced Electromagnetic Propulsion at NASA Glenn Research Center," AIAA paper 2005-4227.
[15]Peterkin, R.E. Jr., Frese, M.H., "MACH: A Reference Manual-First Edition," Air Force Research Laboratory, Phillips Research Site.
[16]Mikellides, I.G., "Theoretical Modeling and Optimization of Ablation-Fed Pulsed Plasma Thrusters," Ph.D. Thesis, The Ohio State University, September 1999.
[17]Kamhawi, H., "Experimental and Theoretical Investigation of Pulsed Plasma Thrusters," Ph.D. Thesis, The Ohio State University, June 2002.
[18]Haag, T.W., "Thrust Stand For Pulsed Plasma Thruster," Rev. *Sci. Instrum 68 (5)*, May 1997, pp. 2060-2067.
[19]Solbes, A., and Vondra, R.J., "Performance Study of a Solid Fuel-Pulsed Electric Microthruster," J. Spacecraft, Vol. 10, NO. 6, June 1973.
[20]Knoepfel, H., "Pulsed High Magnetic Fields," North Holland Publishing Company, London, 1970.
[21]Turchi, P.J., "Directions for Improving PPT Performance," IEPC Paper 97-038.

Table 1. High energy PPT *(HEPPT2)* Test Matrix.

PPT Energy J	Thruster Capacitance		
	100 μF	180 μF	260 μF
100	Yes	Yes	Yes
200	Yes	Yes	Yes
300	Yes	Yes	Yes
450	-	Yes	Yes
700	-	-	Yes

Table 2. PPT capacitors charging voltage magnitudes for the different thruster capacitances and energy levels, "*" denotes capacitance/energy levels that were not tested due to the 2500 V capacitor rating limit.

Capacitance, μF	Pulsed Plasma Thruster Energy				
	100 J	200 J	300 J	450 J	700 J
	Capacitors Charging Voltage, V				
100	1414	2000	2449*	3000*	3741*
180	1054	1491	1826	2236	2788*
260	877	1240	1519	1861	2320

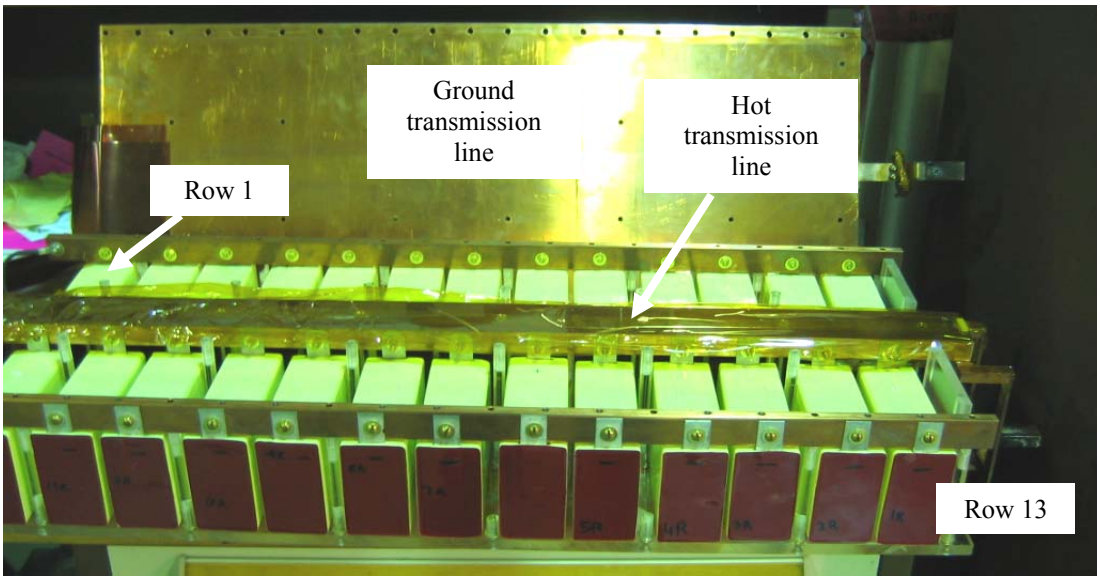

Figure 1. Picture of partially disassembled *HEPPT2* showing the 13 rows of capacitors.

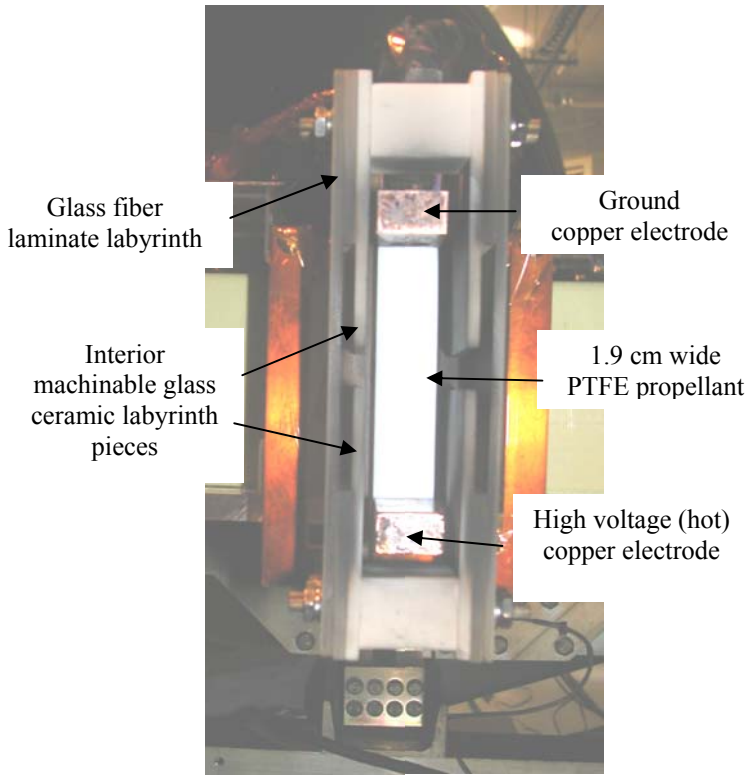

Figure 2. Picture of the inter-electrode region of *HEPPT2*.

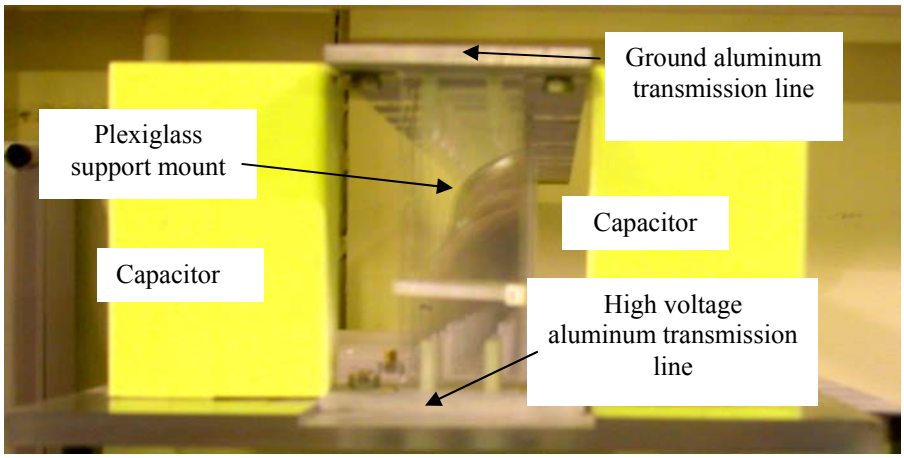

Figure 3. Backview picture of *HEPPT1b* showing the ground and hot transmission lines, capacitors, and plexiglass supporting mount.

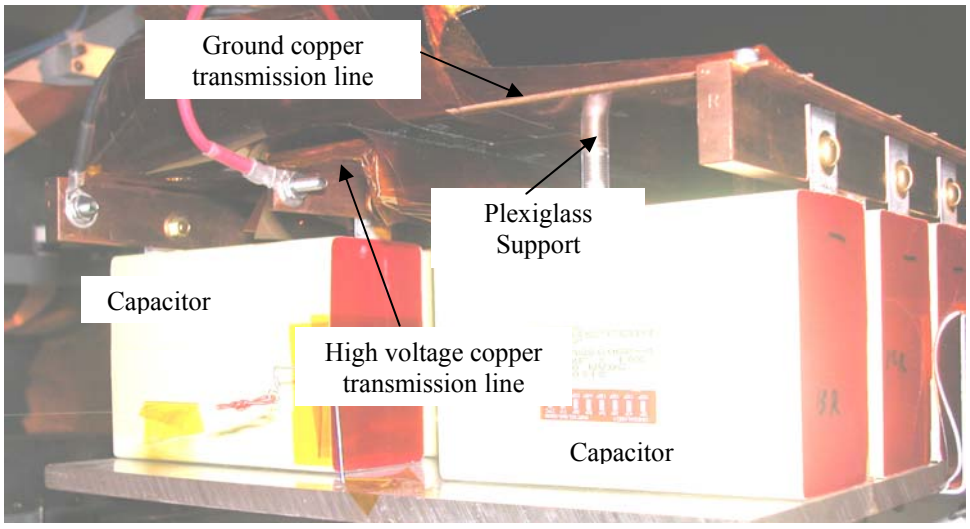

Figure 4. Backview picture of *HEPPT2* showing the copper transmission lines, capacitors, and plexiglass supporting mounts.

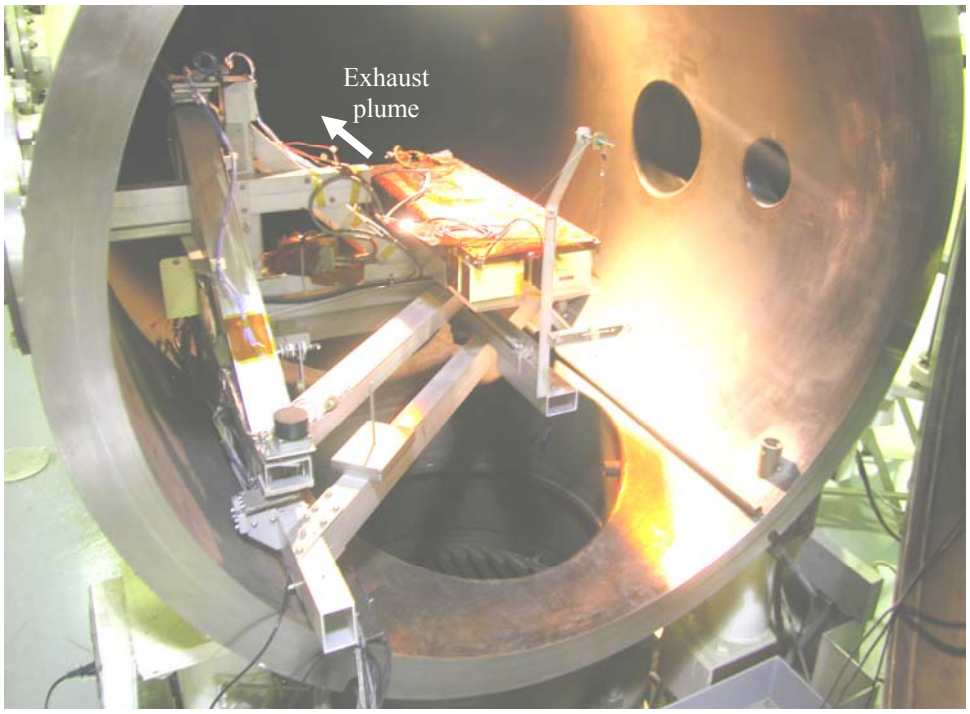

Figure 5. Picture of *HEPPT2* mounted on the PPT thrust stand in VF-3 at NASA GRC.

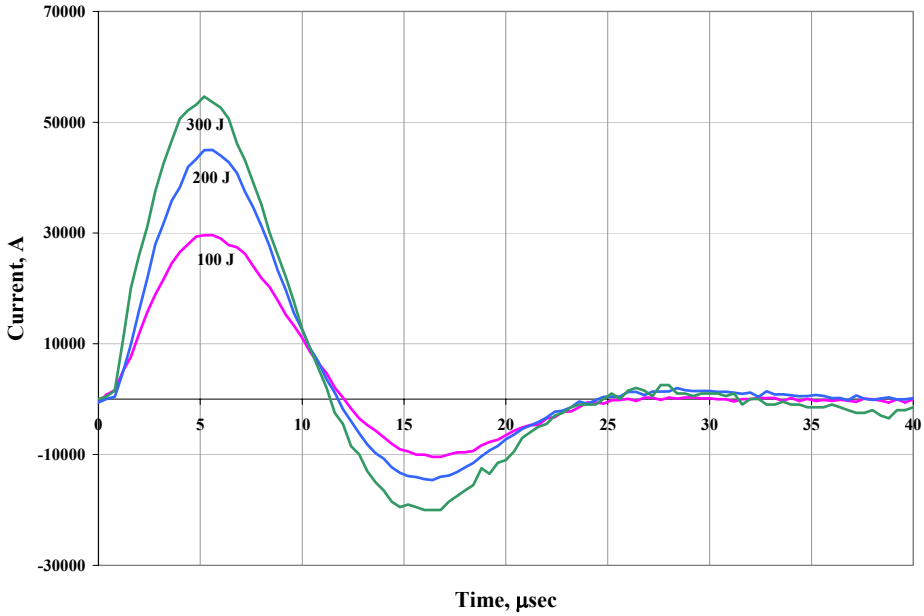

Figure 6. Discharge current waveforms for *HEPPT2* for a thruster capacitance of 100 µF.

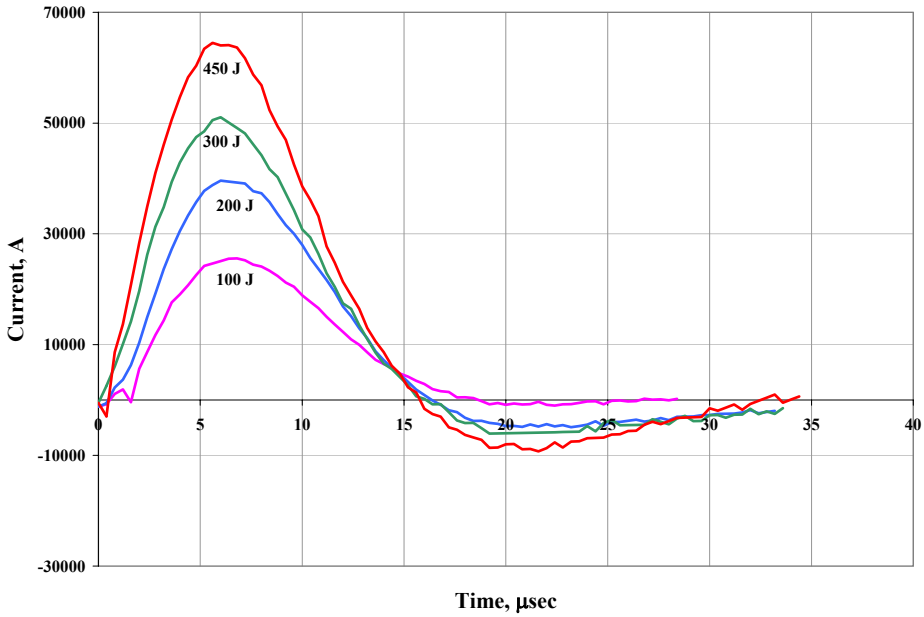

Figure 7. Discharge current waveforms for *HEPPT2* for a thruster capacitance of 180 µF.

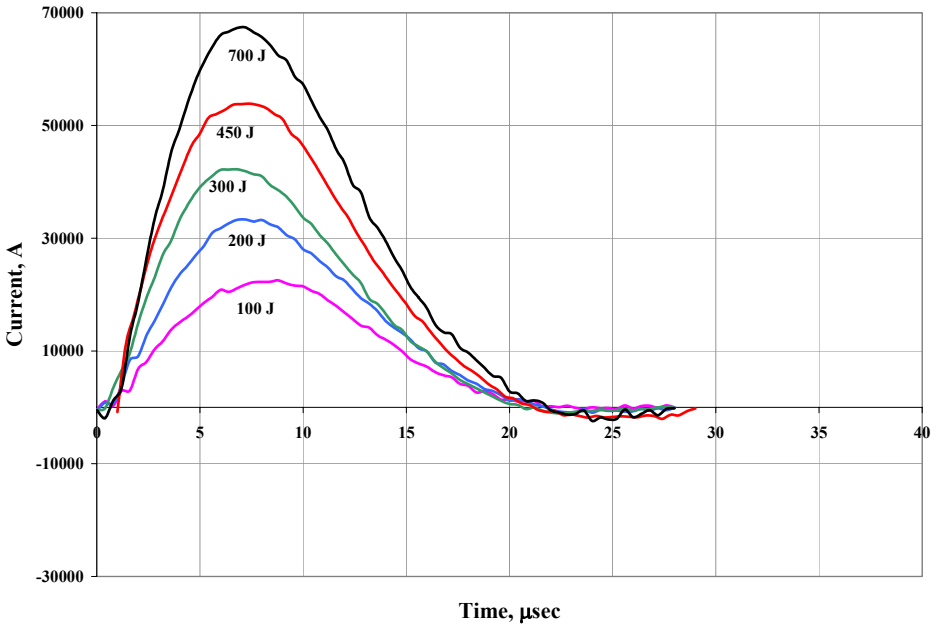

Figure 8. Discharge current waveforms for *HEPPT2* for a thruster capacitance of 260 µF.

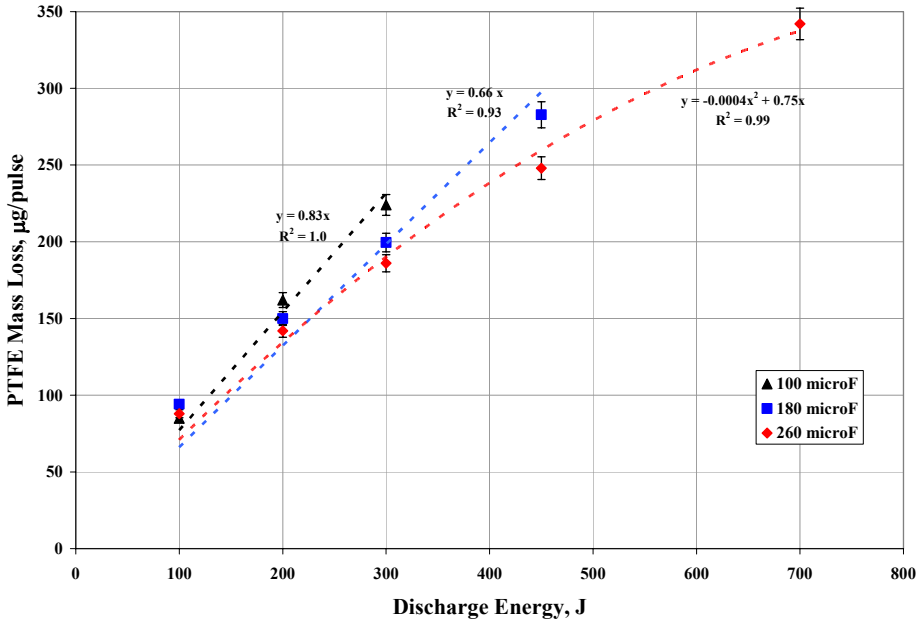

Figure 9. *HEPPT2* PTFE mass loss magnitudes for discharge energy levels between 100 J and 700 J.

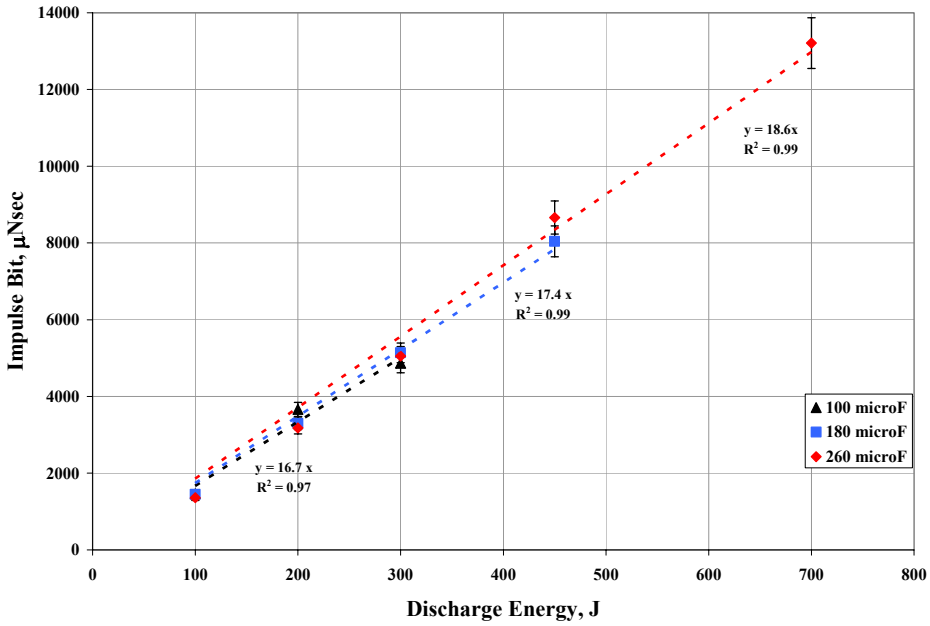

Figure 10. *HEPPT2* impulse-bit magnitudes for discharge energy levels between 100 J and 700 J.

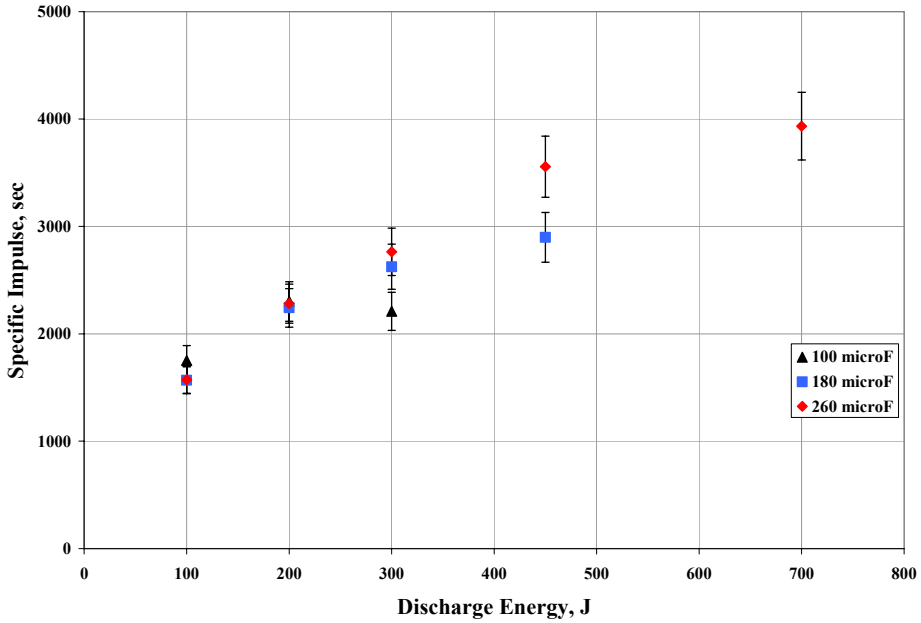

Figure 11. *HEPPT2* specific impulse magnitudes for discharge energy levels between 100 J and 700 J.

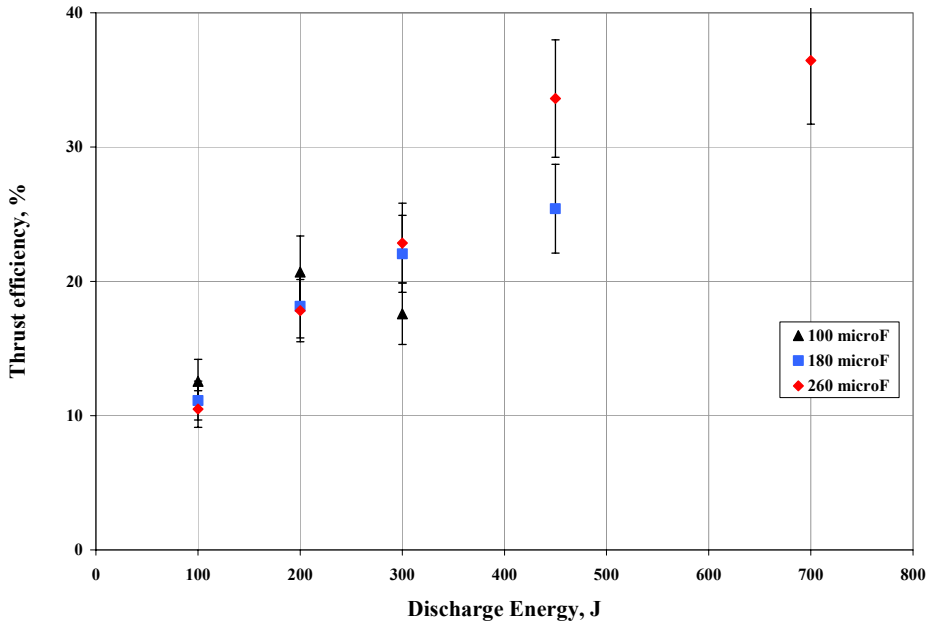

Figure 12. *HEPPT2* thrust efficiency magnitudes for discharge energy levels between 100 J and 700 J.

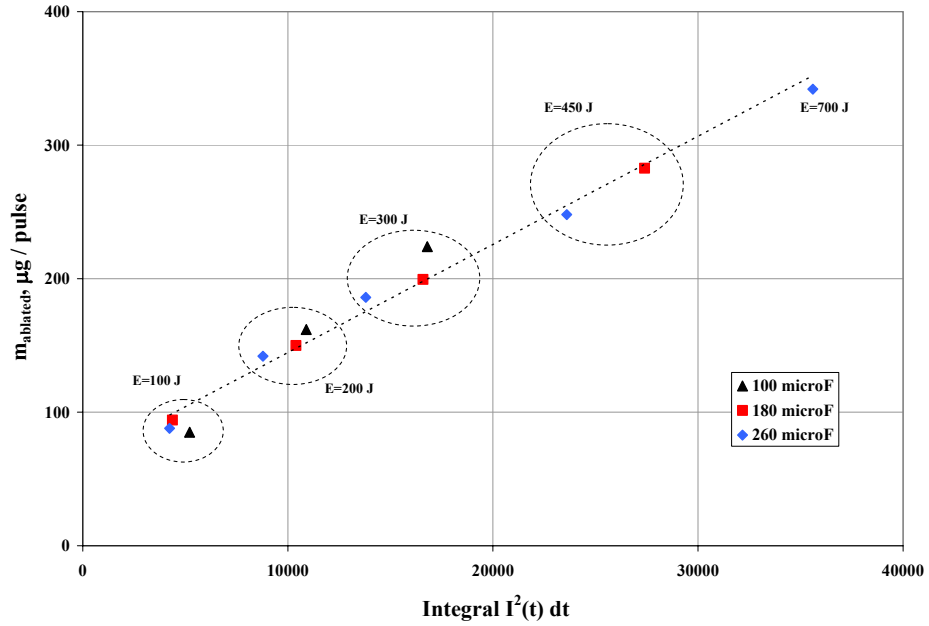

Figure 13. PTFE ablated mass vs. $\int I^2(t)\,dt$ for discharge energy levels between 100 J and 700 J.